Received 2 August 2024; accepted 23 August 2024. Date of publication 29 August 2024; date of current version 11 September 2024.
Digital Object Identifier 10.1109/OJCOMS.2024.3451661

On the Channel Activity Detection in LoRaWAN Networks

LORENZO VANGELISTA (Senior Member, IEEE), AND GIANCARLO CALVAGNO (Member, IEEE)

Department of Information Engineering, University of Padua, 35131 Padua, Italy

CORRESPONDING AUTHOR: L. VANGELISTA (e-mail: lorenzo.vangelista@unipd.it)

The work of Lorenzo Vangelista was supported by the PNRR Research Activities of the Consortium Interconnected North-Est Innovation Ecosystem (iNEST) funded by the European Union Next-GenerationEU Piano Nazionale di Ripresa e Resilienza (PNRR)–Missione 4 Componente 2, Investimento 1.5–D.D.1058 23/06/2022 under Grant ECS_00000043.

ABSTRACT In this paper, we consider the problem of detecting the channel activity in LoRaWAN networks. To improve the medium access performance, recent implementations of the chipsets for LoRaWAN end nodes are offering a feature called Channel Activity Detection (CAD), as the first step toward the implementation of the Carrier Sense Multiple Access (CSMA) in LoRaWAN networks. The algorithm underlying the CAD is at the moment left undisclosed. In this paper, we propose a possible implementation of the CAD algorithm; we then evaluate its performance in an additive white Gaussian noise (AWGN) channel, and we find the performance being completely satisfactory and matching the one of the undisclosed algorithm. The results we find are encouraging the community to include the CAD feature in open source implementations of a LoRaWAN receiver.

INDEX TERMS LoRaWAN, LoRa, low power wide area networks, CSMA.

I. INTRODUCTION

LOW POWER Wide Area Networks (LPWAN) [1] recently emerged as a paradigm for massive Internet of Things (IoT) applications. These applications involve a large number of devices, known as End Nodes (ENs), spread over a wide area, sending small, infrequent packets of information. Two technologies have gained the largest market share in LPWAN: LoRaWAN [2], which operates primarily in unlicensed frequency bands, and NB-IoT [3], which uses licensed frequency bands.

In this paper, we focus on LoRaWAN. Specifically, we address the scalability of LoRaWAN networks and, in particular, a mechanism called Channel Activity Detection (CAD) to enhance it.

The scalability issue of LoRaWAN networks has been identified early on, as noted in studies such as [4], and it remains a topic of ongoing investigation (see, for example, [5]). Considerable research (e.g., [6] and [7]) has been dedicated to optimizing the parameters of a specific algorithm, known as Adaptive Data Rate (ADR) (see [8]), which runs on the back-end of a LoRaWAN network (the Network Server, see below) to improve its capacity.

However, the primary cause of poor scalability in LoRaWAN networks is the channel access mechanism, which for most ENs is based on pure Aloha. Research on this issue to improve the performance of LoRaWAN networks is currently very active, as evidenced by studies such as [9], [10], and [11]. In particular, using a Carrier Sense Multiple Access (CSMA) seems to be very promising (see Section VIII of [12] for details and the very recent papers [13], [14], [15], [16] and [17]).

However, the use of CSMA-based protocols shifts the problem to how CAD can be performed in LoRaWAN networks. This issue is not trivial, as the usual approach of measuring the power in the channel fails completely. This is because LoRa modulation (the physical layer of LoRaWAN networks) typically operates at negative Signal-to-Noise Ratios (SNR). Simple power measurement on the channel is ineffective since, at negative SNR, the signal we wish to detect is below the noise level. Given that LoRa modulation is a spread-spectrum-like modulation, despreading is necessary to increase the SNR level and detect the possible presence of the modulated signal. Semtech, the company that owns the patents on LoRa modulation and produces the majority of LoRa chipsets, has introduced a type of CAD function in some LoRa EN chips (such as the SX1276/77/78/79 transceivers [18]) specifically for packet preamble detection, although they have not disclosed the details of its implementation, as expected.

Interestingly enough, the use of this CAD limited to the preamble of a packet is actually mandated by the LoRa Alliance, the organization that produces and maintains the LoRaWAN specification, for a very different purpose than CSMA, i.e., enabling relays on LoRaWAN networks [19].

Recent work by the Wireless And Networked Distributed Sensing Research Group (WANDS), affiliated with the School of Computer Science and Engineering (SCSE) at Nanyang Technological University (NTU), Singapore [20], proposed the use of CAD provided in Semtech chipsets for a more comprehensive detection of channel activity (see [11] and [21]). In their study [20], the WANDS research group reports two key findings:

- The Semtech "CAD can also detect payload chirps with satisfactory performance. Specifically, it achieves more than 95% precision in detecting the occupancy of an ongoing transmission". Note that a very similar statement is made in [11] and [21].
- The power consumption of the chip during CAD is significantly lower compared to its power consumption during transmission.

In fact, the Semtech SX1276 chip datasheet [18] reports the following:

> "The modem searches for a correlation between the radio captured samples and the ideal preamble waveform."

A very high-level description of a possible solution for CSMA can be found in the paper [21]. Another paper on CSMA in LoRaWAN networks is [22]. Despite the title, the paper deals mainly with CSMA and the backoff algorithm associated with it; it does not provide any detail on how to actually perform the CAD, except referring to the Semtech implementation of CAD on their chipsets. Furthermore, the authors say

> "However, their listening or detection period went on for the whole packet, unlike CAD, which only detects the message preamble."

This sentence is in stark contrast with the CAD algorithm we propose in our paper since our algorithm detects the packet throughout its entire duration, including the payload. We note that the preamble is always supposed to be a minimal part of the packet, and a CAD algorithm that works on the preamble alone is inevitably highly suboptimal, potentially raising some doubts on the results presented in [22]. However, we remark that this paper does not deal with the CSMA in LoRaWAN (which can come in many variants) but with the basic building block required for CSMA, that is, the CAD.

It should be noted that several papers (e.g., [23] and [24]) focus on the search for the preamble, the first part of a LoRaWAN packet with a specific structure designed to detect the start of a packet and align receivers in time and frequency. The algorithms proposed in these papers are not directly applicable for channel activity detection in LoRaWAN. This limitation arises because these algorithms heavily rely on the structure of the preamble, whereas detection in LoRaWAN may also need to consider the payload part of the packet. Additionally, packet synchronization in these algorithms is computationally intensive, as their scope extends to time and frequency synchronization. In contrast, CAD aims to simply detect the presence of a packet.

It is very well known that CSMA is used in several other systems, and one could think of borrowing a channel activity detection algorithm from one of those systems. Limiting ourselves to radio standards, we should cite the IEEE 802.11 [25] standard (commonly referred to as Wi-Fi™) and the IEEE 802.15.4 standard (commonly used in ZigBee™ [26] systems). Referencing to the latest consolidated version of the IEEE 802.11 standard [25], the sentence

> "The ED threshold shall be ≤ -80dBm for TX power $>$ 100 mW, -76dBm for 50 mW $<$ TX power $\leq$ 100 mW, and -70 dBm for TX power $\leq$ 50 mW"

clearly shows how the energy of the received signal (ED stands for Energy Detection) is used and then simply compared to a threshold. Referring then to the latest consolidated version of IEEE 802.15.4 [27] as used in ZigBee [26], according to [28]

> "Energy detection (ED) is used to measure the level of energy in the frequency band of interest at a sensor node. Depending on the strength of energy, the sensor nodes can take appropriate actions, in order to get good performance. A common example of ED is the CCA (clear channel assessment) that is normally performed before packet transmission. This technique is applied in CSMA/CA (Carrier Sense Multiple Access with Collision Avoidance) protocols. If the energy level is below a certain threshold, then the radio starts transmission, otherwise, it backs off to avoid packet collision. CCA threshold is critical for communication performance."

As one can immediately realize, since the LoRa modulation is working below the level of noise (see [1, pag.71]), that is, with a negative signal-to-noise ratio, the sensing mechanisms for CSMA as proposed in other systems, such as the ones previously discussed, cannot work: they would result in a channel always sensed as occupied as the level of signal, even if present, is below that of the noise. As a consequence, the problem considered in this paper is new with respect to other systems.

The main contributions of this paper are as follows:

- a novel, simple and effective algorithm for the CAD in LoRaWAN networks; this algorithm is designed to be utilized in open-source implementations of LoRaWAN receivers, such as the one described in [29], offering

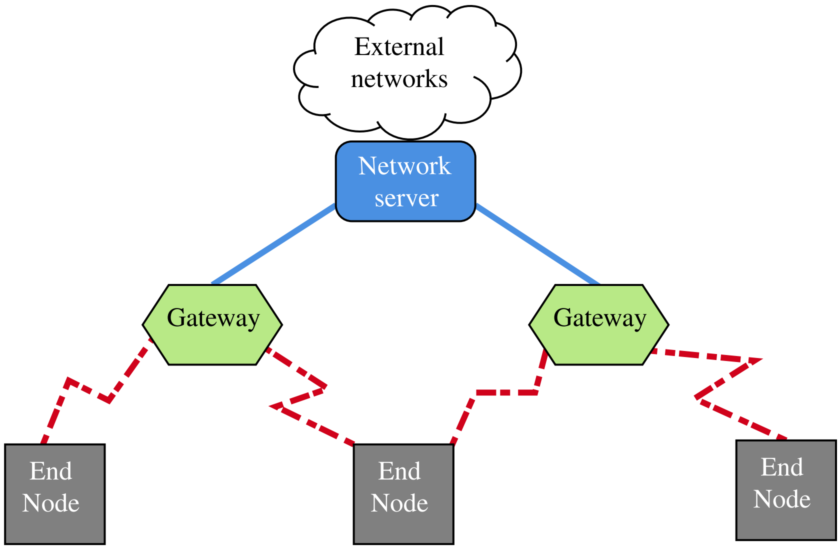

FIGURE 1. A simplified architecture of a LoRaWAN network. The links in read are using the LoRa modulation as physical layer.

a valuable alternative to the undisclosed algorithm proposed in [18];
- a numerical evaluation of the above mentioned algorithm in an AWGN channel, matching the results of the paper [20].

The paper is organized as follows. In Section II we provide the description of the system as far as the CAD is concerned; we also provide the working points, in terms of SNR for each Spreading Factor, to be used for the evaluation of the CAD. In Section III we provide a description of the simple and effective CAD algorithm that we propose in this paper and in Section IV we numerically evaluate its performance. Section V provides some concluding remarks and envisions possible future works.

II. SYSTEM DESCRIPTION

The LoRaWAN network, in principle, is made up of three major entities (see Figure 1) described in the following paragraph.

- End Nodes (EN): the devices at the edge of the network sensing data and sending them via radio to the Network Server (see below) as well as receiving data via radio and acting according to them (e.g., executing a command with related parameters).
- Gateways (GW): the devices relaying the data to and from the Network Server and the ENs, trough the radio interface on the ENs side and usually via a cabled connection (ADSL, fiber etc.) on the Network Server (see below) side.
- Network Server (NS): the back-end entity responsible both for the control (admission of the ENs, billing, etc.) plane and the user plane, i.e., to forward and receive the ENs data to and from external networks.

It can be seen from the above description that the topology of a LoRaWAN network is a "star of stars" one. It can be seen as well that the LoRaWAN network is "cell-free", that is, a packet sent from an EN (e.g., the one in the center of Figure 1) can be picked up from more than one gateway; each gateway forwards the packet to the NS, which is charge to de-duplicate the packets. Clearly, the LoRaWAN network is packet-based.

In LoRaWAN networks the ENs are of three types (called "classes"), whose details are provided in the following paragraph.

- Class A: the EN when sending packet to the network uses a pure Aloha protocol and listen to possible signal from the network for a short period after sending the uplink packet. In all remaining time the receiver (and most of the circuitry) of the EN is switched off. The vast majority of the EN in LoRaWAN networks are Class A devices, since in this class one can minimize the power consumption. Class A devices are supposed to be battery powered.
- Class B: the EN is sending and receiving packets according to a schedule broadcast by the GW and set up by the NS. The access mechanism for this class of devices is very similar to a slotted Aloha one. The Class B devices are rarely used since their operation (including listening in their assigned downlink slot from the network) entails a higher power consumption. Class B devices are supposed to be battery powered.
- Class C: the EN is continuously listening for possible downlink packets, except when it is transmitting an uplink packet. The devices of Class C are attached to the main power and are used in the, relatively few, cases when a low latency in the reaction to a command from the network is required.

For a complete description of a LoRaWAN network, we refer the reader to [30] and the recent survey [31]. In these references more details are given on the different classes of

ENs, on the components of the Network Server (including the Join Server and the Application Server), on the MAC layer, etc.

In this paper, we deal with the Physical Layer of LoRaWAN, i.e., LoRa. In the following we provide a description of the LoRa Physical layer, focusing on the part relevant for this paper.

Throughout the paper, we adopt the notation of [32]. We denote by $u(t)$ the unit step function, and we will make use of the indicator function defined as

$$g_T(t) = \begin{cases} 1, & 0 \le t < T; \\ 0, & \text{elsewhere.} \end{cases}$$

We consider the complex envelope of a LoRa signal centered at zero frequency, which is defined as

$$i(t) = \gamma \sum_n x(t - nT_s; a_n) g_{T_s}(t - nT_s) \tag{1}$$

where a_n is the symbol transmitted in the time interval $[nT_s, (n+1)T_s)$, and

$$x(t; a) = e^{j2\pi Bt\left(\frac{a}{M} - \frac{1}{2} + \frac{Bt}{2M} - u\left(t - \frac{M-a}{B}\right)\right)}. \tag{2}$$

The passband modulated signal centered at f_0 is then $s(t) = \Re\mathfrak{e}(i(t)e^{j2\pi f_0 t})$. The parameters used in the above Equations (1) and (2) are defined in Table 1.

Equation (1) considers a sequence of symbols with undefined length. However, in the LoRaWAN system the symbols are transmitted by an EN in packets.

The structure of the packet is shown in Figure 2, and is made of:

- 8 *upchirps*, that is, 8 symbols with $a_n = 0$ (shown in green in Figure 2);
- 2 symbols carrying the *sync word* equal to `0x34` for public networks, which is the main focus of this paper (shown in red in Figure 2);
- 2.25 *downchirps*, that is, 2.25 symbols with $a_n = 0$ and having the term $+\frac{Bt}{2M}$ in Eq. (2) replaced by $-\frac{Bt}{2M}$, producing a linear negative frequency slope (shown in green in Figure 2); for this portion of the signal we define

$$x_-(t; a) = e^{j2\pi Bt\left(\frac{a}{M} - \frac{1}{2} - \frac{Bt}{2M} - u\left(t - \frac{M-a}{B}\right)\right)}; \tag{3}$$

- a generic number N of information bearing symbols (shown in blue in Figure 2).

Taking a generic LoRaWAN packet, starting at T_{start}, we can write the complex envelope $p(t)$ of the signal carrying the packet as in equation (4) at the bottom of next page, where N is the number of symbols in the payload part of the packet.

An EN detects the presence of a LoRaWAN packet by processing the received signal in a time window $[T_{obs,s}, T_{obs,e})$. In the following of the paper the length of the observation window T_{obs} is set to $T_{obs} = T_{obs,e} - T_{obs,s} = M_0 T_s$, with $M_0 = 2$. Note that the CAD in [18] utilizes a much longer observation window, i.e., $T_{obs} = 8T_s$. We remark that, differently from [18], we cannot take advantage of the particular structure of the packet, since we cannot assume that we have any information about the relative position of our observation window with respect to the start of the packet (in [18] instead, it is assumed that $T_{obs,s} < T_{start}$).

TABLE 1. Notation and parameter definitions.

Symbol	definition	comments
SF	Spreading Factor (SF)	$SF \in \{7, 8, \ldots, 12\}$
M	2^{SF}	
B	$B = 125$ KHz	nominal bandwidth
T_c	$T_c = 1/B$	chip period
T_s	$T_s = M\,T_c$	symbol period
a_n	symbol transmitted in time interval $[nT_s, (n+1)T_s)$	$a_n \in \{0, \ldots, 2^{SF}-1\}$
P_S	passband signal power	
γ	$\gamma = \sqrt{2P_s}$	we assume $\gamma = 1$ unless otherwise stated
T_{start}	starting time of a packet	
T_{end}	ending time of a packet	
$T_{obs,s}$	starting time of the observation window	
$T_{obs,e}$	ending time of the observation window	
T_{obs}	duration of the observation window	$T_{obs} = T_{obs,e} - T_{obs,s}$
N	number of symbols in the payload part of the packet	
M_0	number of LoRa Symbols used for the CAD	$T_{obs} = M_0\,T_s$

In the following of the paper we consider three possible cases regarding the position of the observation window with respect to the packet. The selection is not exhaustive but encompasses, in our opinion, the most relevant cases.

`clear` This case refers to the situation $T_{obs,e} < T_{start}$ or, equivalently,

$$T_{obs,s} < T_{start} - 2T_s.$$

We assume that before the packet under observation there are no packets for at least T_{obs} seconds. In this case, the CAD subsystem should ideally report that the channel is clear, and we define the probability that the CAD subsystem reports a busy channel as the probability of false alarm P_{false}.

`fuzzy` This case refers to the situation where

$$T_{start} - T_{obs} < T_{obs,s} < T_{start},$$

that is, when the observation window includes a portion of the preamble. In this case, the CAD

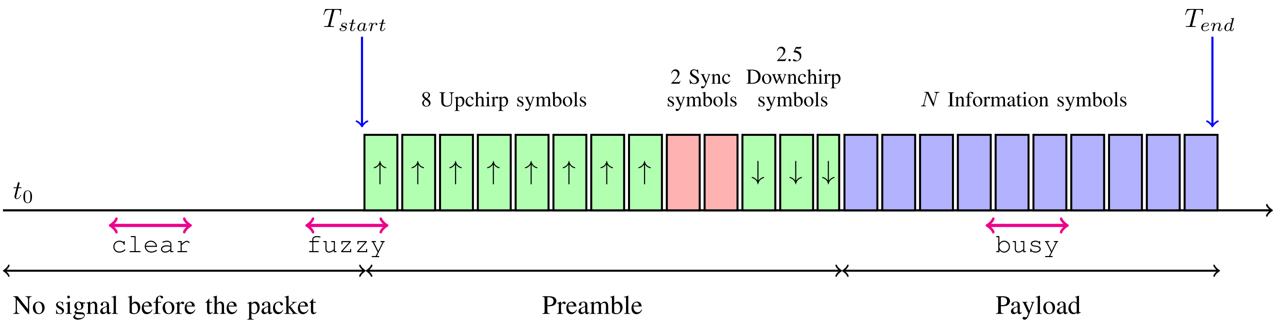

FIGURE 2. **The reference scenario for the performance assessment: an example.**

subsystem should ideally report that the channel is occupied and we define the probability that the CAD subsystem reports a clear channel as the probability of false alarm P_{miss}.

`busy` This case refers to the situation where

$$T_{start} \leq T_{obs,s} < T_{start} + NT_s + 10.25T_s,$$

that is, when the transmitter is active in the entire observation window. In this case, the CAD subsystem should ideally report that the channel is occupied, and also in this case the key performance indicator is P_{miss}.

In the following, according to the implementation in [18], we consider a payload length of 40 symbols, that is, $N = 40$ and we also assume a Complex Additive White Gaussian Noise channel with noise power σ^2, denoted $\mathcal{CAWGN}(\sigma^2)$.

A. SNR AND WORKING POINT

In this subsection, we outline the key parameters that will be utilized for performance evaluation throughout the rest of the paper. These parameters are defined according to the current literature on the LoRa Physical Layer. We compile and define them here for two reasons: first, there are slight variations in their definitions across different papers; second, we want to provide the reader with clear definitions to facilitate the reproduction of our results.

In [33], the signal-to-noise ratio Γ is defined as

$$\Gamma = \frac{E_s/T_s}{N_0 B} = \frac{E_S}{N_0\, 2^{SF}}.$$

Comparing Equation (2) with Equation (1) of [33], we recognize that

$$\gamma = \sqrt{\frac{E_S}{2^{SF}}}, \tag{5}$$

and therefore, using our notation, we obtain

$$\Gamma = \frac{\gamma^2}{N_0}, \tag{6}$$

where $N_0 = kTB$, with $k = 1,38065 \times 10^{-23}$ the Boltzmann constant and $T = 290\,\mathrm{K}$ the temperature.

To compute P_{false} and P_{miss}, we need to determine the SNR-based operation area for LoRa modulation in the LoRaWAN network. To this purpose, in Appendix A we have derived the SNR values that ensure a packet error rate (PER) equal to 10%, which is the operating point described in [34, Sec. 7.2.4.1]. These values are listed in Table 2, together with the range within which we are going to provide the performance of the CAD subsystem.

III. GENERIC CAD ALGORITHM

In this section, we tackle the main problem addressed by our paper. We describe in more detail the CAD problem and propose a couple of algorithms which are more general than those existing in the literature.

In our setting, a non-coherent reception is employed, lacking the elements for implementing a coherent reception, such as the knowledge of where the preamble is and if there is a preamble in our observation window.

In [35], an algorithm is proposed to optimize the LoRa preamble detection. The problem considered in this paper

$$\begin{aligned} p(t) = &\sum_{n=0}^{7} x(t - T_{start} - nT_s; 0) g_{T_s}(t - T_{start} - nT_s) + \sum_{n=8}^{9} x(t - T_{start} - nT_s; a_n) g_{T_s}(t - T_{start} - nT_s) \\ &+ \sum_{n=10}^{11} x_-(t - T_{start} - nT_s; 0) g_{T_s}(t - T_{start} - nT_s) + x_-(t - T_{start} - 12T_s; 0) g_{T_s/4}(t - T_{start} - 12T_s) \\ &+ \sum_{n=12}^{12+N} x(t - T_{start} - nT_s - T_s/4; a_n) g_{T_s}(t - T_{start} - nT_s - T_s/4) \end{aligned} \tag{4}$$

TABLE 2. Minimum SNR and range of SNR values for the evaluation of the CAD subsystem.

SF	Minimum SNR (dB)	SNR Range (dB)
7	-7	$[-7, -5]$
8	-10	$[-10, -8]$
9	-13	$[-13, -11]$
10	-16	$[-16, -14]$
11	-19	$[-19, -17]$
12	-22	$[-22, -20]$

is substantially different since we would like to detect a generic unknown sequence of LoRa symbols, whereas in [35] the sequence is known. In fact, we note that the so-called preamble in [35] is not the LoRaWAN preamble, but a sequence of LoRa symbols $a_n = 0$. Furthermore, we note that the algorithm in [35] assumes perfect timing, perfect knowledge of the power of the signal, and perfect knowledge of the power of the noise. These assumptions are quite unrealistic for the scenario we are considering in this paper. However, the algorithm in [35], can be conveniently modified in the following way.

- Instead of looking at the first bin of the DFT (corresponding to the transmitted symbol $a_n = 0$), we may look for the highest peak of the magnitude of the DFT output and assume that the corresponding symbols is transmitted. This assumption is obviously not valid, since the sample timing of the receiver with respect to the "true" timing of the received signal is not known. That may cause the received symbol to have several bins with large values (actually distributed with a "$sinc(\cdot)$" shape). However, since we would like to keep the complexity of the algorithm low, we do not see other possibilities. As a matter of fact, sampling the received signal at $T_c/2$ allows us to mitigate the adverse effect of this assumption.
- We assume all the DFT bins except the one having the largest magnitude are made of noise. This hypothesis suffers from the same problems of the previous assumption and the same mitigation strategy is used.
- The largest magnitude of the DFT is compared with an appropriate threshold and if it is greater than the threshold, then the channel activity is declared.
- Since there is no symbol synchronization between the receiver and the transmitter, which may cause a smearing and lowering of the DFT magnitude peaks, to prevent missing activity detection the CAD procedure tries $N_{Step} = 8$ demodulations with starting times distributed uniformly in a symbol time interval.

A detailed description of the algorithm that we propose for channel activity detection is provided by the pseudo-code reported in Algorithm 1.

As mentioned above, to mitigate the effects of timing misalignment, the algorithm works at the sampling rate $T_c/2$, and it performs $N_{Step} = 8$ demodulations considering a sliding observation window to contrast the lack of symbol synchronization. The input of the algorithm is the parameter α, which is used to define the detection threshold, and the observation window d, which is a portion of the received signal of length $2T_s$. In Appendix B we describe a procedure to estimate the value to be assigned to the parameter α for a desired value of the false detection probability P_{false} in the absence of transmissions.

Algorithm 1: Channel Activity Detection

```
Data: α, d_{T_c/2}(n) : T_{obs,s} ≤ n T_c/2 < T_{obs_s} + 2T_s
Result: Success or Fail in the detection
N_Step ⟵ 8;
Step ⟵ M/N_Step ;
S ⟵ 0;
for ℓ ∈ {0, 1} do
    for k ∈ {0, ..., N_Step − 1} do
        for m ∈ {0, ..., M − 1} do
            y[m] = d_{T_c/2}(k Step + 2m + ℓ) e^{−j2π m²/(2M)} ;
        Y = DFT(y);
        θ = α mean{|Y|};
        M_Y = max{|Y|};
        if M_Y > θ then
            S ⟵ S + 1;
if S ≥ 1 then
    Channel activity has been detected;
else
    No channel activity has been detected;
```

Algorithm 1 performs the demodulation using a downchirp and therefore it does not allow the activity detection in case the observation window falls in correspondence of the 2.25 downchirps in the preamble. If we would like to detect also the downchirps of the preamble, it is necessary to modify the procedure considering both downchirp and upchirp demodulation. In such a case, the channel activity detection algorithm has to be modified as described by the pseudo-code in Algorithm 2. The drawback of this version is an obvious increase in complexity, but also a smaller sensitivity, as we will see analyzing the numerical results in Section IV.

IV. NUMERICAL RESULTS

In this section, we present the results of the simulation campaign that was carried out to assess the performances of the proposed algorithms. In our experiments we set $T_{start} = 10T_s$ and the payload length to $N = 40$. Without loss of generality, we assume the following settings for the 3 cases described in Section II:

`clear` $T_{obs,s} = 2T_s$ and $T_{obs_e} = T_{obs,s} + M_0 T_s = 4T_s$;
`fuzzy` $T_{obs,s} = 9T_s$ and $T_{obs_e} = T_{obs,s} + M_0 T_s = 11T_s$;
`busy` $T_{obs,s} = 32T_s$ and $T_{obs_e} = T_{obs,s} + M_0 T_s = 34T_s$.

Algorithm 2: Up/Down Channel Activity Detection

Data: α, $d_{T_c/2}(n)$: $T_{obs,s} \leq n\,T_c/2 < T_{obs_s} + 2T_s$

Result: Success or Fail in the detection

$N_{Step} \longleftarrow 8$;

$Step \longleftarrow M/N_{Step}$;

$S \longleftarrow 0$;

for $\ell \in \{0, 1\}$ **do**

  for $k \in \{0, \ldots, N_{Step} - 1\}$ **do**

    for $m \in \{0, \ldots, M - 1\}$ **do**

      $\mathbf{y}_d[m] = d_{T_c/2}(k\,Step + 2m + \ell)\, e^{-j2\pi \frac{m^2}{2M}}$;

      $\mathbf{y}_u[m] = d_{T_c/2}(k\,Step + 2m + \ell)\, e^{j2\pi \frac{m^2}{2M}}$;

    $\mathbf{Y}_d = DFT(\mathbf{y}_d)$; $\mathbf{Y}_u = DFT(\mathbf{y}_u)$;

    $\theta_d = \alpha\, \mathrm{mean}\{|\mathbf{Y}_d|\}$; $\theta_u = \alpha\, \mathrm{mean}\{|\mathbf{Y}_u|\}$;

    $M_{Yd} = \max\{|\mathbf{Y}_d|\}$; $M_{Yu} = \max\{|\mathbf{Y}_u|\}$;

    if $M_{Yd} > \theta_d$ or $M_{Yu} > \theta_u$ **then**

      $S \longleftarrow S + 1$;

if $S \geq 1$ **then**

  Channel activity has been detected;

else

  No channel activity has been detected;

We are aware that a greater variety of intermediate cases can actually occur; however, for the sake of simplicity, we decided to focus on these three.

A. SIMULATION CONFIGURATION

We assume that the input of the CAD algorithm is the signal

$$d(t) = p(t - \tau_c T_c - \tau_s T_s), \tag{7}$$

where τ_c accounts for the time misalignment between the transmitter and the receiver, and τ_s for the absence of symbol synchronization. In the simulations we consider values of τ_c and τ_s randomly selected in the intervals $(-\frac{1}{8}, \frac{1}{8})$ and $(-\frac{1}{4}, \frac{1}{4})$, respectively. The amplitude of these intervals were chosen to span half the sampling period $T_c/2$ and half the symbol period T_s, so that there is a complete desynchronization between the transmitter and the receiver. The values of the information symbols a_n in the packet were chosen randomly in the alphabet $\{0, 1, \ldots, M - 1\}$, and for each experiment we chose a different set of symbols. The values of the thresholds θ, θ_d and θ_u were set according to the estimation procedure provided in Appendix B, where we also describe the computation of the parameter α in terms of the false alarm probability P_{false}.

B. ASSESSING THE PERFORMANCES OF ALGORITHM 1

A first set of simulations were carried out setting the parameter α such that the probability of false alarm P_{false} in the `clear` case results about 1%. We conducted 10,000,000 experiments for both $SF = 7$ and $SF = 10$ using Algorithm 1 and found the results shown in Tables 3 and 4, respectively. In the tables we report the P_{false} probability for the `clear` case and the P_{miss} probabilities for the `fuzzy` and `busy` cases, together with the corresponding 95% confidence intervals (CI).

TABLE 3. Results and 95% CI for Algorithm 1 with *SF* = 7.

	`clear`: P_{false}	`fuzzy`: P_{miss}	`busy`: P_{miss}
SNR $= -7$ dB	0.010070 $\pm 6.2\times10^{-5}$	0.06666 $\pm 1.5\times10^{-4}$	0.005111 $\pm 4.4\times10^{-5}$
SNR $= -5$ dB	0.010129 $\pm 6.2\times10^{-5}$	0.001125 $\pm 2.1\times10^{-5}$	0.0000014 $\pm 7\times10^{-7}$

TABLE 4. Results and 95% CI for Algorithm 1 with *SF* = 10.

	`clear`: P_{false}	`fuzzy`: P_{miss}	`busy`: P_{miss}
SNR $= -16$ dB	0.011034 $\pm 6.5\times10^{-5}$	0.10543 $\pm 1.9 \times \times10^{-4}$	0.010240 $\pm 6.2\times10^{-5}$
SNR $= -14$ dB	0.010985 $\pm 6.5\times10^{-5}$	0.001944 $\pm 2.7\times10^{-4}$	0.0000032 $\pm 1.1\times10^{-6}$

Notice that as the SNR increases, the probability of missing detection P_{miss} reduces dramatically both in the `busy` and the `fuzzy` cases.

As a side result, we mention that, in agreement with what stated in the final comments to Appendix B, the value of the parameter α that we employed for the simulations depends on the spreading factor *SF* but does not depend on the SNR. This result testify the robustness of the proposed algorithm with respect to different noise scenarios.

C. ASSESSING THE PERFORMANCES OF ALGORITHM 2

A second set of simulations were performed in the same scenario as in Section IV-B but using Algorithm 2. The corresponding results for $SF = 7$ and $SF = 10$ are reported in Tables 5 and 6, respectively.

As expected, when using Algorithm 2 in place of Algorithm 1, to obtain a similar probability of false alarm P_{false} in the `clear` case, we need to increase the value of α (and therefore of the thresholds), since the number of the noise samples increases from M to $2M$. As a consequence the probability of missing detection P_{miss} in the `busy` case increases significantly. This is the unavoidable price to be payed for allowing the detection of the downchirps in the preamble. Considering that there are only 2.25 downchirps symbols in the entire packet, a cost benefit analysis of using Algorithm 2 in place of the simpler and more sensitive Algorithm 1 should be carried out case by case, depending on the applications and on the number N of information symbols in the packet.

D. ASSESSING THE RECEIVER OPERATING CHARACTERISTICS

The parameter α that sets the thresholds in Algorithm 1 and Algorithm 2 can be used to trade-off between the P_{false} and P_{miss} probabilities. As the value of α increases, the

TABLE 5. Results and 95% CI for Algorithm 2 with $SF = 7$.

	clear: P_{false}	fuzzy: P_{miss}	busy: P_{miss}
SNR $= -7$ dB	0.010165 $\pm 6.2\times10^{-5}$	0.09449 $\pm 1.8\times10^{-4}$	0.011055 $\pm 6.5\times10^{-5}$
SNR $= -5$ dB	0.010248 $\pm 6.2\times10^{-5}$	0.002300 $\pm 3.0\times10^{-5}$	0.0000081 $\pm 1.8\times10^{-6}$

TABLE 6. Results and 95% CI for Algorithm 2 with $SF = 10$.

	clear: P_{false}	fuzzy: P_{miss}	busy: P_{miss}
SNR $= -16$ dB	0.009964 $\pm 6.2\times10^{-5}$	0.14143 $\pm 2.2\times10^{-4}$	0.022632 $\pm 9.2\times10^{-5}$
SNR $= -14$ dB	0.009937 $\pm 6.2\times10^{-5}$	0.003705 $\pm 3.8\times10^{-5}$	0.0000183 $\pm 2.7\times10^{-6}$

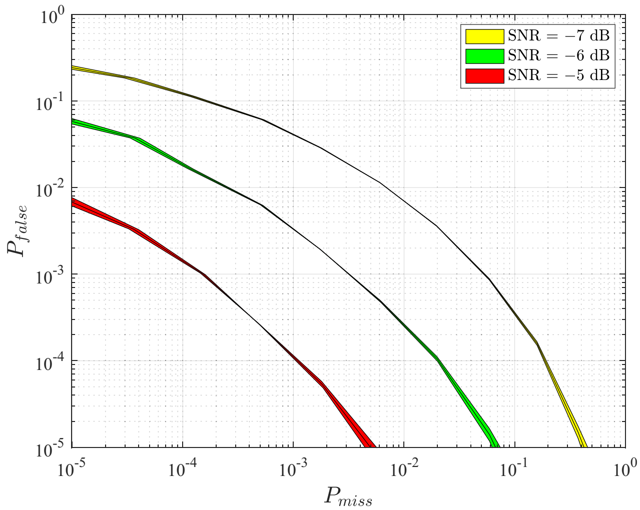

FIGURE 3. P_{miss} vs P_{false} CI plots for $SF = 7$.

probability P_{false} in the `clear` case decreases while the probability P_{miss} in the `busy` case increases.

A third set of simulations was set up to find the relation between the P_{false} and P_{miss} probabilities, i.e., the Receiver Operating Characteristics (ROC). By varying the value of the parameter α we obtained several (P_{false}, P_{miss}) pairs for different values of the SNR. The corresponding ROC curves are shown in Figure 3 and Figure 4 for $SF = 7$ and $SF = 10$, respectively. The plots show the 95% confidence intervals in shades of different colors for the different values of the SNR.

The results shown in these figures were obtained using Algorithm 1, but curves with similar behavior are obtained in case of using Algorithm 2.

We can observe that our findings confirm that the proposed algorithm can detect the presence of a LoRaWAN packet with $P_{false} < 1\%$ in the `clear` case and $P_{miss} < 1\%$ in the `busy` case even in the most unfavorable SNR scenarios.

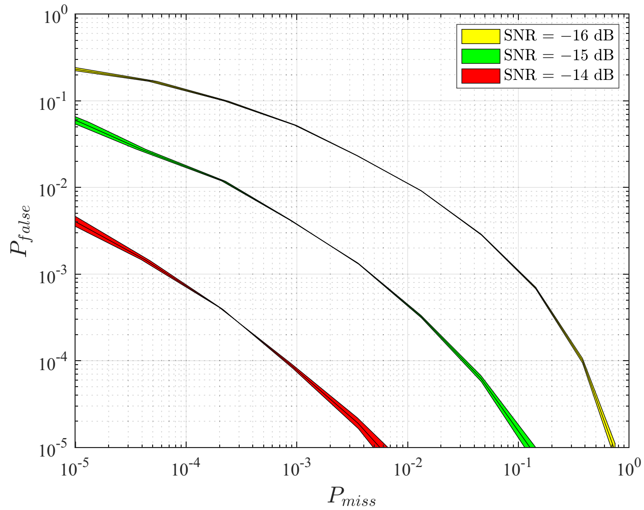

FIGURE 4. P_{miss} vs P_{false} CI plots for $SF = 10$.

An additional remarkable observation is that the computational complexity of the proposed algorithm is quite low.

V. CONCLUSION AND FUTURE WORK

In this paper we proposed a novel, simple and effective CAD algorithm. The algorithm is more general than those currently available in literature as it detects the channel activity considering the whole LoRa packet and not just the preamble of the packet. We evaluated its performance in an AWGN channel, and we found that it matches very well that of the undisclosed algorithm implemented in [18].

We plan, as future work, to further assess the performance of the proposed algorithm by including several other impairments, such as a fading channel.

The relevance of this research is clear as one considers that the introduction of CSMA in LoRa networks is becoming widespread, both in academic literature and in real-world networks.

APPENDIX A
OPERATING POINT FOR THE CAD SUBSYSTEM

Assuming $SF = 10$ and a target packet error rate of 10% for a payload of 20 bytes, we can calculate the airtime of the packet using the airtime calculator [36] as 0.4526 s. The duration T_s of a symbol for $SF = 10$ and a bandwidth $B = 125$ kHz is $T_s = 2^{SF}/B = 8.192$ ms; a packet with a payload of 20 bytes accounts for approximately $Q_{20-sym} \approx 55$ symbols and $Q_{20-bits} \approx 550$ bits. Denoting as P_{bit} the bit error probability, we can approximate the packet error rate $P_{packet,20,SF=10}$ for a packet with a payload of 20 bytes and $SF = 10$ as

$$P_{packet,20,SF=10} = 1 - (1 - P_{bit})^{Q_{20-bits}}. \tag{8}$$

Having imposed that $P_{packet,20,SF=10} = 10\%$ we obtain from Eq. (8) $P_{bit} \approx 2 \cdot 10^{-4}$ which corresponds from Figure 1 of [33] to $\Gamma = \Gamma_{10} \approx -16$ dB. We then investigate the behavior of the CAD subsystem for $SF = 10$ in the range $\Gamma_{10} \in [-16, -14]$ dB.

To obtain the sensitivity values for the other $SFs \neq 10$, for the purpose of this paper, we note that, as one can intuitively argue from the fact that increasing SF by 1 we almost double the energy per symbol, to calculate the minimum SNR reaching the sensitivity we start from the one calculated for $SF = 10$ and we derive the others adding or subtracting 3dB at every step. The results are shown in Table 2.

APPENDIX B ESTIMATION OF THE THRESHOLD

To the estimate the threshold values, we made the following analysis. We consider two extreme values for SF, that is, 7 and 10 ($SF = 11$ and $SF = 12$ cannot be used in certain regions, for example, in the USA). For $SF = 7$ the highest ratio between the signal power and the noise one is -5 dB, that is, 0.31, while for $SF = 10$ it is -14 dB, that is, 0.04. We can then reasonably say that the signal $p(t)$ is more of a noise than the actual signal. We then approximate the signal $p(t)$ as $\mathcal{CN}\big(0, \sigma^2\big)$. When considering then the fact that the DFT is a unitary operator, i.e., it preserves the energy of its input, we see that $|\mathbf{Y}[m]|$ is a Rayleigh distributed random variable with scale parameter $\sigma/\sqrt{2}$.

Without any knowledge about the possible received signal, the most reasonable target for the CAD algorithm is to require that the probability of false detection in the absence of transmissions, P_{false}, is lower than an assigned value p_0. From this constraint we can estimate the value of the threshold θ to be used in the CAD algorithm. In case of no transmission, a false detection corresponds to having at least one DFT bin magnitude greater that the threshold θ. Modeling the DFT bin magnitudes $|\mathbf{Y}[m]|$, $m = 1, 2, \ldots, M$ as independent and identically distributed Rayleigh random variables, and considering that the total number of DFT bins considered in the CAD algorithm in $L = N_{Step}M$, we obtain the constraint

$$P_{false} = 1 - (P(|\mathbf{Y}[m]| \leq \theta))^L \leq p_0,$$

or, equivalently,

$$P(|\mathbf{Y}[m]| \leq \theta) \geq (1 - p_0)^{1/L}.$$

Since the cumulative distribution function of a Rayleigh random variable Y with scale parameter σ is

$$F_Y(y) = P(Y \leq y) = 1 - e^{-y^2/(2\sigma^2)}, \quad \text{for} \quad y \in [0, \infty),$$

we get the following inequality

$$1 - e^{-\theta^2/(2\sigma^2)} \geq (1 - p_0)^{1/L},$$

i.e.,

$$\theta \geq \sigma\sqrt{-2\log\big(1 - (1 - p_0)^{1/L}\big)}.$$

For a Rayleigh random variable, $\sigma = \sqrt{\frac{2}{\pi}}\,\mathbb{E}[Y]$, and therefore we finally obtain

$$\theta \geq \sqrt{-\frac{4}{\pi}\log\big(1 - (1 - p_0)^{1/L}\big)}\,\mathbb{E}[Y].$$

This inequality can be used to set the minimum threshold θ_0 to be employed in the proposed CAD algorithm in terms of the given value of p_0 and of $\mathbb{E}[Y]$, which can be estimated by computing the average value of the available DFT bin magnitudes $|\mathbf{Y}[m]|$, $m = 1, 2, \ldots, M$.

As examples, in case $p_0 = 0.01$, for $M = 128$ (i.e., $SF = 7$) we get $\theta_0 = 3.83\,\mathbb{E}[Y]$, while for $M = 1024$ (i.e., $SF = 10$) we get $\theta_0 = 4.16\,\mathbb{E}[Y]$. These results are in very good agreement with those obtained by means of computer simulations, since we found that to obtain a 1% probability of false detection in the absence of transmissions, we had to set $\theta_0 = 3.91\,\mathbb{E}[Y]$ and $\theta_0 = 4.23\,\mathbb{E}[Y]$ for $M = 128$ and $M = 1024$, respectively.

Note that the parameter $\alpha = \sqrt{-\frac{4}{\pi}\log(1 - (1 - p_0)^{1/L})}$ is independent of the intensity of the noise. Moreover, also in case of channel activity, the value $\mathbb{E}[Y]$ can be estimated as the average of all the DFT bin magnitudes, since for a LoRa signal only one DFT bin is nonzero and its contribution to the average value is therefore negligible.

ACKNOWLEDGMENT

The authors would like to thank the reviewers for their useful comments and suggestions that helped improving the article. This manuscript reflects only the Authors' views and opinions, neither the European Union nor the European Commission can be considered responsible for them.

REFERENCES

[1] B. S. Chaudhari and M. Zennaro, *LPWAN Technologies for IoT and M2M Applications*. London, U.K.: Acad. Press, 2020.

[2] C. Pham, A. Bounceur, L. Clavier, U. Noreen, and M. Ehsan, "Radio channel access challenges in LoRa low-power wide-area networks," in *LPWAN Technologies for IoT and M2M Applications*. London, U.K.: Acad. Press, 2020.

[3] M. Bakri Hassan, A. E. Sayed, R. A. Mokhtar, R. A. Saeed, and B. S. Chaudhari, "NB-IoT: concepts, applications, and deployment challenges," in *LPWAN Technologies for IoT and M2M Applications*. London, U.K.: Acad. Press, 2020.

[4] O. Georgiou and U. Raza, "Low power wide area network analysis: Can LoRa scale?" *IEEE Wireless Commun. Lett.*, vol. 6, no. 2, pp. 162–165, Apr. 2017.

[5] M. Jouhari, E. M. Amhoud, N. Saeed, and M.-S. Alouini, "A survey on scalable LoRaWAN for massive IoT: Recent advances, potentials, and challenges," 2022, *arXiv:2202.11082*.

[6] D. Garlisi, I. Tinnirello, G. Bianchi, and F. Cuomo, "Capture aware sequential waterfilling for LoRaWAN adaptive data rate," *IEEE Trans. Wireless Commun.*, vol. 20, no. 3, pp. 2019–2033, Mar. 2021.

[7] J. Lyu, D. Yu, and L. Fu, "Analysis and optimization for large-scale LoRa networks: Throughput fairness and scalability," *IEEE Internet Things J.*, vol. 9, no. 12, pp. 9574–9590, Jun. 2022.

[8] "SX1276." Semtech. Accessed: Mar. 21, 2023. [Online]. Available: https://lora-developers.semtech.com/documentation/tech-papers-and-guides/understanding-adr

[9] L. Beltramelli, A. Mahmood, P. Österberg, and M. Gidlund, "LoRa beyond ALOHA: An investigation of alternative random access protocols," *IEEE Trans. Ind. Informat.*, vol. 17, no. 5, pp. 3544–3554, May 2021.

[10] C. Zhong and A. Springer, "Analysis of a novel media access control protocol for LoRa," *IEEE Internet Things J.*, vol. 10, no. 1, pp. 341–356, Jan. 2023.

[11] A. Gamage, J. Liando, C. Gu, R. Tan, M. Li, and O. Seller, "LMAC: Efficient carrier-sense multiple access for LoRa," *ACM Trans. Sen. Netw.*, vol. 19, no. 2, pp. 1–27, Feb. 2023. [Online]. Available: https://doi.org/10.1145/3564530

[12] P. Gkotsiopoulos, D. Zorbas, and C. Douligeris, "Performance determinants in LoRa networks: A literature review," *IEEE Commun. Surveys Tuts.*, vol. 23, no. 3, pp. 1721–1758, 3rd Quart., 2021.

[13] C. Shao and O. Muta, "When LoRaWAN meets CSMA: Trends, challenges, and opportunities," *IEEE Internet Things Mag.*, vol. 7, no. 1, pp. 90–96, Jan. 2024.

[14] B. Gu, Z. Lin, Z. Huang, S. Gong, Z. Su, and M. Guizani, "CORA: Channel occupancy-aware resource allocation in LoRa wireless networks," *IEEE Trans. Veh. Technol.*, early access, Jul. 9, 2024, doi: 10.1109/TVT.2024.3425459.

[15] J. Mhatre, A. Lee, H. Lee, and R. Aygun, "Design and implementation of multithreaded CAD-enabled LoRa simulator for massive IoT," in *Proc. 18th Int. Conf. Ubiquitous Inf. Manage. Commun. (IMCOM)*, 2024, pp. 1–7.

[16] J. Mhatre, A. Lee, H. Lee, and T. N. Nguyen, "DDPG_CAD: Intelligent channel activity detection scheduling in massive IoT LoRaWAN," in *Proc. IEEE 10th Int. Conf. Netw. Softw. (NetSoft)*, 2024, pp. 248–252.

[17] H. Zhang, H. Liu, Z. Tao, and Y. Zhang, "LoRa network protocol design based on CSMA/CA with asynchronous downlink mode," in *Proc. 4th Int. Conf. Digit. Signal Comput. Commun. (DSCC)*, 2024, Art. no. 132140W. [Online]. Available: https://doi.org/10.1117/12.3033369

[18] "SX1276." Semtech. Accessed: Mar. 21, 2023. [Online]. Available: https://www.semtech.com/products/wireless-rf/lora-connect/sx1276

[19] "LoRaWAN® relay specification," LoRa Alliance, Freemont, CA, USA, document TS011-1.0.0, Oct. 2022.

[20] *LMAC: Efficient CSMA for LoRa Wireless And Networked Distributed Sensing (WANDS)*, Nanyang Technol. Univ., Singapore, Accessed: Mar. 21, 2023. [Online]. Available: https://wands.sg/lmac/

[21] A. Gamage, J. C. Liando, C. Gu, R. Tan, and M. Li, "LMAC: Efficient carrier-sense multiple access for LoRa," in *Proc. 26th Annu. Int. Conf. Mobile Comput. Netw.*, New York, NY, USA, 2020. [Online]. Available: https://doi.org/10.1145/3372224.3419200

[22] K. Kamonkusonman and R. Silapunt, "Channel activity detection with the modified Backoff algorithm for LoRaWAN," in *Proc. 18th Int. Conf. Elect. Eng./Electron., Comput., Telecommun. Inf. Technol. (ECTI-CON)*, 2021, pp. 86–89.

[23] C. Bernier, F. Dehmas, and N. Deparis, "Low complexity LoRa frame Synchronization for ultra-low power software-defined radios," *IEEE Trans. Commun.*, vol. 68, no. 5, pp. 3140–3152, May 2020.

[24] L. Vangelista and A. Cattapan, "Start of packet detection and synchronization for LoraWAN modulated signals," *IEEE Trans. Wireless Commun.*, vol. 21, no. 6, pp. 4608–4621, Jun. 2022.

[25] *IEEE Standard for Information Technology–Telecommunications and Information Exchange Between Systems-Local and Metropolitan Area Networks–Specific Requirements-Part-11: Wireless LAN Medium Access Control (MAC) and Physical Layer (PHY) Specifications*, IEEE Standard 802.11-2020, (Revision of IEEE Std 802.11-2016), Feb. 2021.

[26] S. Farahani, *ZigBee Wireless Networks and Transceivers*. Amsterdam, The Netherlands: Elsevier, 2008. [Online]. Available: http://dx.doi.org/10.1016/B978-0-7506-8393-7.X0001-5

[27] *IEEE Standard for Low-Rate Wireless Networks*, IEEE Standard 802.15.4-2020, (Revision of IEEE Std 802.15.4-2015), Jul. 2020.

[28] D. Yuan, S. S. Kanhere, and M. Hollick, "Instrumenting wireless sensor networks—A survey on the metrics that matter," *Pervasive Mobile Comput.*, vol. 37, pp. 45–62, Jun. 2017. [Online]. Available: https://www.sciencedirect.com/science/article/pii/S1574119216302802

[29] J. Tapparel, O. Afisiadis, P. Mayoraz, A. Balatsoukas-Stimming, and A. Burg, "An open-source LoRa physical layer prototype on GNU radio," in *Proc. IEEE 21st Int. Workshop Signal Process. Adv. Wireless Commun. (SPAWC)*, 2020, pp. 1–5.

[30] A. Yegin et al., "LoRaWAN protocol: specifications, security, and capabilities," in *LPWAN Technologies for IoT and M2M Applications*. London, U.K.: Acad. Press, 2020.

[31] C. Milarokostas, D. Tsolkas, N. Passas, and L. Merakos, "A comprehensive study on LPWANs with a focus on the potential of LoRa/LoRaWAN systems," *IEEE Commun. Surveys Tuts.*, vol. 25, no. 1, pp. 825–867, 1st Quart., 2023.

[32] M. Chiani and A. Elzanaty, "On the LoRa modulation for IoT: Waveform properties and spectral analysis," *IEEE Internet Things J.*, vol. 6, no. 5, pp. 8463–8470, Oct. 2019.

[33] T. Elshabrawy and J. Robert, "Closed-form approximation of LoRa modulation BER performance," *IEEE Commun. Lett.*, vol. 22, no. 9, pp. 1778–1781, Sep. 2018.

[34] "System reference document (SRdoc); technical characteristics for low power wide area networks chirp spread spectrum (LPWAN-CSS) operating in the UHF spectrum below 1 GHz, Version 1.1.1," Eur. Telecommun. Stand. Inst., Sophia Antipolis, France, Rep. 103 236, Apr. 2018. [Online]. Available: https://www.etsi.org/deliver/etsi_tr/103500_103599/103526/01.01.01_60/tr103526v010101p.pdf

[35] J.-M. Kang, "LoRa preamble detection with optimized thresholds," *IEEE Internet Things J.*, vol. 10, no. 7, pp. 6525–6526, Apr. 2023.

[36] "LoRaWAN airtime calculator." Things Network. Accessed: Apr. Jul. 2023. [Online]. Available: https://www.thethingsnetwork.org/airtime-calculator

LORENZO VANGELISTA (Senior Member, IEEE) received the Laurea and Ph.D. degrees in electrical and telecommunication engineering from the University of Padua, Padua, Italy, in 1992 and 1995, respectively, where he is currently a Full Professor. He subsequently joined the Transmission and Optical Technology Department, CSELT, Turin, Italy. From December 1996 to January 2002, he was with Telit Mobile Terminals, Trieste, Italy. In May 2003, he was with Microcell A/S, Copenhagen, Denmark. In July 2006, he joined the Worldwide Organization, Infineon Technologies, as a Program Manager. From October 2006 to October 2021, he was an Associate Professor of telecommunication with the Department of Information Engineering, University of Padua. His research interests include signal theory, multicarrier modulation techniques, cellular networks, and the Internet of Things connectivity with a special focus on low power wide area networks.

GIANCARLO CALVAGNO (Member, IEEE) received the Laurea degree in Ingegneria Elettronica and the Doctorate degree in Ingegneria Elettronica e dell'Informazione from the University of Padua, Italy, in 1986 and 1990, respectively, where he has been an Associate Professor with the Department of Information Engineering since 1998. From 1988 to 1990, he was with the Coordinated Science Laboratory, University of Illinois at Urbana-Champaign as a Visiting Scholar. From 1990 to 1998 he was a Ricercatore with the Department of Information Engineering, University of Padua. He has been involved in several national and European research projects on image and video processing and coding. His main research interests are in the areas of digital signal processing, signal reconstruction, and multidimensional signal analysis and coding, with special emphasis on the transmission of images and video sequences.

Open Access funding provided by 'Università degli Studi di Padova' within the CRUI CARE Agreement